Inorganic Chemistry
Cite This: Inorg. Chem. 2018, 57, 7805−7814
Article
pubs.acs.org/IC

Lanthanide-benzophenone-3,3′-disulfonyl-4,4′-dicarboxylate Frameworks: Temperature and 1-Hydroxypyren Luminescence Sensing and Proton Conduction

Wen-Wen Zhang,[†] Yu-Ling Wang,*[,†] Qingyou Liu,[‡] and Qing-Yan Liu*[,†]

[†]College of Chemistry and Chemical Engineering, Key Laboratory of Functional Small Organic Molecule of Ministry of Education, Jiangxi Normal University, Nanchang, Jiangxi 330022, P. R. China

[‡]Institute of Geochemistry, Chinese Academy of Sciences, Guiyang 550081, P. R. China

Supporting Information

ABSTRACT: The benzophenone-3,3′-disulfonyl-4,4′-dicarboxylic acid (H_4−BODSDC) ligand and compounds, $\{(H_3O)[Ln(BODSDC)(H_2O)_2]\}_n$ (Ln = Tb(**1**), Eu(**2**), and Gd(**3**)), were synthesized and structurally characterized. The lanthanide centers are bridged by the carboxylate groups of $BODSDC^{4-}$ ligands to give a one-dimensional (1D) chain. The 1D chains are connected by the $BODSDC^{4-}$ ligands to yield a three-dimensional (3D) structure featuring 1D channels. The lanthanide ions are efficiently sensitized by the $BODSDC^{4-}$ ligand with an appropriate triplet excited state to generate characteristic Tb(III) and Eu(III) emissions in Tb(**1**) and Eu(**2**), respectively. Thus the binary compound, $\{(H_3O)[Tb_{0.93}Eu_{0.07}(BODSDC)(H_2O)_2]\}_n$ (abbreviated as $Tb_{0.93}Eu_{0.07}$-BODSDC), was achieved for use as a ratiometric temperature sensor. The ratio values of Tb(III) emission at 544 nm (I_{Tb}) and Eu(III) emission at 616 nm (I_{Eu}) for $Tb_{0.93}Eu_{0.07}$-BODSDC linearly vary with temperature over a wide range, which indicates that the $Tb_{0.93}Eu_{0.07}$-BODSDC is a thermometer for ratiometric fluorescence sensing of temperature. Additionally, Tb(**1**) is a fluorescent probe for detecting 1-hydroxypyrene (1-HP) by luminescence quenching. The uncoordinated sulfonate oxygens exposed on the channel surfaces serve as the binding sites for 1-HP. Finally, the enrichment of the solvent water molecules in the channels decorated by high-density hydrophilic sulfonate groups resulted in a high proton conductivity for Tb(**1**).

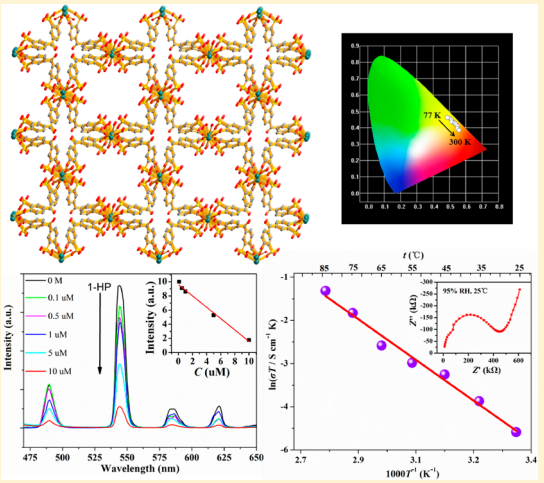

INTRODUCTION

Metal−organic frameworks (MOFs) made of metals coordinated to organic ligands are a unique class of functional materials exhibiting numerous important applications that originated from the metal centers or functional organic ligands as well as the well-defined porosity.[1] By deliberately selecting inorganic and organic building units, the magnetism, electricity, and luminescence endowed by inorganic metal ions and organic linkers can be introduced into the MOFs, leading to new kinds of functional materials and devices.[2] Because the lanthanides have unique fluorescence properties derived from the abundant 4f−4f transitions, the lanthanide-based MOFs (Ln-MOFs) are fascinating candidates for the preparation of fluorescence-sensing devices.[3] Recently, the Ln-MOF-based luminescence sensors display the recognition properties for cations and anions,[4] small molecules,[5] temperature,[6] and pH.[7] On the contrary, the organic ligands as an important component for MOFs play a vital role in the synthesis of MOFs and thus the properties. In particular, for Ln-MOFs, the lanthanide luminescence needed to be sensitized by the organic ligands due to the Laporte forbidden f−f transitions.[8] Because of the oxyphilic preference of lanthanide ions, the carboxylate ligands are extensively used for the construction of the Ln-MOFs.[9] The organic ligands bearing the sulfonate group are seldom applied to the preparation of the MOFs because the sulfonate group is a weak ligating group,[10] which leads to low-robust frameworks. Indeed, some interesting physical properties such as gas separation and fluorescence sensing can be introduced by incorporation of the sulfonate group.[11] The bifunctional ligand containing carboxylate oxygens with strong coordination ability and sulfonate oxygens with weak coordination ability simultaneously is an interesting class of ligand, although the MOFs based on the sulfonate-carboxylate ligands are relatively rare.[12] Additionally, the sulfonate-carboxylate ligands are expected to construct a robust sulfonate MOF due to the formation of the strong bonds between the carboxylate oxygen and the metal centers.

Received: April 4, 2018
Published: June 19, 2018

DOI: 10.1021/acs.inorgchem.8b00865
Inorg. Chem. 2018, 57, 7805−7814

Scheme 1. Synthesis of H_4−BODSDC

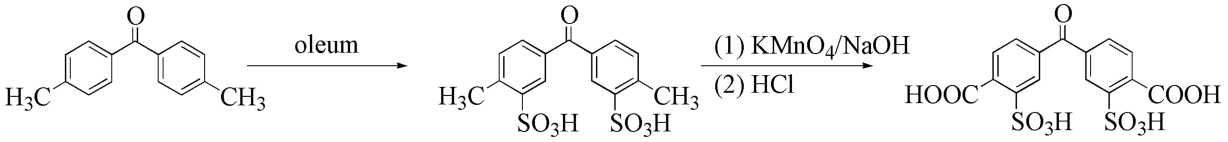

Herein a novel sulfonate-carboxylate ligand, benzophenone-3,3′-disulfonyl-4,4′-dicarboxylic acid (H_4−BODSDC), was prepared. The H_4−BODSDC ligand containing two 2-sulfobenzoate moieties will be an effective component in the design of MOFs. In this contribution, a series of H_4−BODSDC-based Ln-MOFs, $\{(H_3O)[Ln(BODSDC)(H_2O)_2]\}_n$ (Ln = Tb(**1**), Eu(**2**) and Gd(**3**)) and $\{(H_3O)[Tb_{0.93}Eu_{0.07}(BODSDC)(H_2O)_2]\}_n$ (abbreviated as $Tb_{0.93}Eu_{0.07}$-BODSDC), were synthesized. These compounds exhibit 3D frameworks with 1D channels. The Tb(**1**) and Eu(**2**) compounds show temperature-dependent luminescence. The Eu(III)-doped compound $Tb_{0.93}Eu_{0.07}$-BODSDC with two kinds of emitting centers behaves as a ratiometric fluorescence sensor of temperature related to the good sensitization of the organic ligand. The Tb(**1**) compound displays a fluorescence sensing for 1-hydroxypyren (1-HP) with a high antijamming capability and a good proton conduction that were associated with the sulfonate groups on the 1D open channels.

EXPERIMENTAL SECTION

General Instrumentation. IR (KBr pellets, cm^{-1}) measurements were performed on a PerkinElmer Spectrum One FT-IR spectrometer in the range 4000−400 cm^{-1}. ^1H nuclear magnetic resonance (NMR) spectra were recorded with a Bruker AVANCE 400 spectrometer. Thermogravimetric analyses (TGAs) were measured on a PE Diamond thermogravimetric analyzer from 30 to 800 °C at a heating rate of 10 °C/min under a N_2 flow. Powder X-ray diffraction (PXRD) was carried out with a Rigaku Miniflex II powder diffractometer equipped with Cu−Kα radiation (λ = 1.5418 Å). The determination of the metal concentrations in $Tb_{0.93}Eu_{0.07}$-BODSDC was carried out using an inductively coupled plasma (ICP) OES spectrometer (Ultima2, HORIBA Jobin Yvon) with the sample dissolved in concentrated HNO_3. Fluorescence spectra including the decay curves were measured with an Edinburgh FLS980 fluorescence spectrophotometer equipped with an Oxford Instruments liquid nitrogen flow cryostat.

The AC impedance measurements were performed on an Impedance/Gain-Phase analyzer (Solartron SI 1260) by the conventional quasi-four-probe method using gold paste and gold wires (50 μm diameter). Impedance data were collected with an applied potential 100 mV and the frequency ranging from 1 to 1 × 10^6 Hz. Nyquist plots with the real (Z') and imaginary (Z'') parts were generated with the ZView2 software. Fitting of the Nyquist plots gives the proton conductivities. Crystalline samples of Tb(**1**) were compressed as a pellet (2.5 mm diameter, 0.52 mm thickness) under 500 MPa pressure. The exposure of the pellets to temperature and humid environments was performed on an XK-CTS80Z incubator.[4b]

Chemicals. The chemicals employed were obtained from commercial sources. Benzophenone-3,3′-disulfonyl-4,4′-dicarboxylic acid (H_4−BODSDC) was prepared according to Scheme 1.

Synthesis of H_4−BODSDC. The H_4−BODSDC was prepared by a two-step reaction sequence according to Scheme 1.

4,4′-Dimethylbenzophenone (10 g) was added to 30 mL of sulfuric acid fuming (50%), which was refluxed at 120 °C for 7 h and then cooled to room temperature. The reaction mixture was poured into ice water, and 3 g sodium chloride was added to the mixture. The white crude product was precipitated by adding sodium hydroxide into the above mixture. The product of benzophenone-3,3′-disulfonyl-4,4′-dimethyl was recrystallized from ethanol/water solvent (v/v 4:1) and dried at room temperature under vacuum. Yield: 68% based on 4,4′-dimethylbenzophenone.

Benzophenone-3,3′-disulfonyl-4,4′-dimethyl. ^{1}HNMR (400 M, d_6-DMSO, δ): 8.12 (d, 2H), 7.53 (dd, 2H), 7.32 (d, 2H), 2.63 (s, 6H). IR spectrum: 3483 (s), 2202 (w), 1640 (s), 1599 (s), 1557 (w), 1439 (w), 1397 (m), 1386 (m), 1306 (s), 1274 (s), 1260 (s), 1190 (s), 1087 (s), 1030 (s) (O = S═O of − SO_3H group), 977 (m), 924 (w), 844 (w), 827 (w), 806 (w), 756 (m), 727 (w), 714 (w), 706 (m), 674 (m), 631 (s) (C−S), 597 (m), 569 (m), 552 (m), 537 (m), 499 (m), 443 (m).

Sodium hydroxide was slowly added to a solution of 5 g benzophenone-3,3′-disulfonyl-4,4′-dimethyl and 50 mL of deionized water in a flask until the pH value of the mixture was 10. The mixture was refluxed at 90 °C for 1 h, then stood for 1 h. After that, 8.2 g powdered $KMnO_4$ was added to the mixture in small portions. Finally, the mixture was further refluxed at 90 °C for 9 h and filtrated. The concentrated hydrochloric acid was used to acidify the filtrate until the value of the filtrate was about 2. White solid of H_4−BODSDC was obtained after standing 48 h. The final product was dried under vacuum. Yield: 46% based on benzophenone-3,3′-disulfonyl-4,4′-dimethyl.

H_4−BODSDC. ^{1}HNMR (400 M, d_6-DMSO, δ): 7.82−7.71 (m, 4H), 8.15 (d, 2H). IR spectrum: 3598 (s), 3531 (s), 3402 (s), 2934 (s), 2643 (m), 2536 (m), 1970 (w), 1743 (s), 1715 (s), 1672 (s), 1637 (m), 1601 (m), 1556 (w), 1489 (m), 1422 (m), 1381 (m), 1282 (s), 1234 (s), 1135 (s), 1078 (s), 1027 (s), 989 (w), 975 (w), 916 (w), 869 (m), 797 (m), 754 (m), 738 (m), 685 (w), 657 (w), 621 (s), 594 (m), 570 (m), 533 (w), 502 (w), 450 (w).

Synthesis of $\{(H_3O)[Ln(BODSDC)(H_2O)_2]\}_n$ (Ln = Tb(1), Eu(2), and Gd(3)). The three compounds were prepared with a similar process: $Ln(NO_3)_3{\cdot}6H_2O$ (0.1 mmol), H_4−BODSDC (0.1 mmol), and 3 mL H_2O/CH_3CN (v/v 1:2) were mixed in a 25 mL Parr Teflon-lined stainless steel vessel. The vessel was sealed and heated to 85 °C. The temperature was maintained for 4 days; then, the mixture was allowed to cool naturally to obtain crystals. Yield: 39.9% for Tb(**1**); 30.8% for Eu(**2**); 29.1% mg for Gd(**3**). IR spectrum: for Tb(**1**), 3373 (s), 1656 (s), 1578 (s), 1544 (s), 1485 (m), 1430 (s), 1248 (s), 1176 (s), 1080 (s), 1022 (s), 850 (w), 798 (w), 752 (w), 693 (w), 608 (m), 477 (w); for Eu(**2**), 3443 (s), 1669 (w), 1570 (s), 1544 (s), 1488 (m), 1414 (s), 1374(m), 1308 (m), 1250 (s), 1180 (s), 1078 (s), 1028 (s), 968 (m), 853 (m), 795 (m), 756 (m), 680 (w), 622 (m), 497 (w); for Gd(**3**), 3445 (s), 1663 (w), 1578 (s), 1552 (s), 1545 (s), 1487 (m), 1421 (s), 1375 (m), 1316 (m), 1250 (s), 1179 (s), 1074 (s), 1028 (s), 969 (w), 916 (w), 851(s), 799(m), 759 (w), 693 (w), 622 (m), 497 (w).

Synthesis of $\{(H_3O)[Tb_{0.93}Eu_{0.07}(BODSDC)(H_2O)_2]\}_n$. The preparation of the Tb/Eu mixed compound was similar to Tb(**1**) except $Tb(NO_3)_3{\cdot}6H_2O$ (0.1 mmol) was replaced with a mixture of lanthanide salts ($Tb(NO_3)_3{\cdot}6H_2O$ (0.095 mmol) and $Eu(NO_3)_3{\cdot}6H_2O$ (0.005 mmol)). Yield: 32.8%. IR spectrum: 3379 (s), 1650 (s), 1572 (s), 1545 (s), 1487 (s), 1421 (s), 1244 (s), 1172 (s), 1079 (s), 1022 (s), 910 (w), 851 (m), 799 (w), 759 (m), 693 (w), 608 (s), 576 (w), 477 (s). The actual Tb/Eu mole ratio is 0.9289:0.0711 determined by ICP.

Single-Crystal X-ray Diffraction Experiments. X-ray diffraction experiments were carried out at 293(2) K on a Rigaku Oxford SuperNova diffractometer equipped with a Mo−Kα (λ = 0.71073 Å) sealed tube and an Eos detector. The instrument was controlled with CrysAlisPro software package,[13] which was used for collecting the diffraction images, absorption correction, and data reduction. The

DOI: 10.1021/acs.inorgchem.8b00865
Inorg. Chem. 2018, 57, 7805−7814

Table 1. Crystallographic Data for 1−3[a]

	Tb(1)	Eu(2)	Gd(3)
formula	$C_{15}H_{13}O_{14}S_2Tb$	$C_{15}H_{13}O_{14}S_2Eu$	$C_{15}H_{13}O_{14}S_2Gd$
fw	640.29	633.33	620.61
temp (*K*)	293(2)	293(2)	293(2)
cryst syst	monoclinic	monoclinic	monoclinic
space group	*P2/c*	*P2/c*	*P2/c*
Z	4	4	4
a (Å)	19.6142(6)	19.6761(6)	19.6583(11)
b (Å)	16.2865(5)	16.3241(5)	16.3010(8)
c (Å)	9.2476(3)	9.2356(3)	9.2484(5)
α (deg)	90	90	90
β (deg)	98.754(3)	99.061(3)	98.577(5)
γ (deg)	90	90	90
V (Å^3)	2919.70(16)	2929.41(16)	2930.5(3)
D_{calcd} (g·cm^{-3})	1.457	1.436	1.447
μ (mm^{-1})	2.617	2.335	2.452
no. of reflns collected	24401	31071	30520
independent reflns	5975	6002	5999
obsd reflns ($I > 2\sigma(I)$)	5192	5393	5372
F(000)	1248	1240	1244
R[int]	0.0301	0.0395	0.0513
R_1 ($I > 2\sigma(I)$)	0.0255	0.0344	0.0604
wR_2 (all data)	0.0628	0.0950	0.1411
CCDC number	1831920	1831921	1831922

[a] $R_1 = \Sigma||F_o| - |F_c||/\Sigma|F_o|$ and $wR_2 = \{\Sigma[w(F_o^2 - F_c^2)^2]/\Sigma[w(F_o^2)^2]\}^{1/2}$

structures were solved using direct methods (SHELXT-2015)[14] followed by full matrix least-squares refinements against F^2 (SHELXTL-2014).[15] All atoms except for hydrogen atoms are refined with anisotropic thermal parameters. Hydrogen atoms were placed geometrically and refined using the riding model. The location of the disordered hydrated cations in the difference Fourier map was unsuccessful. The highly disordered guest solvent molecules were treated by SQUEEZE program[16] to generate a set of solvent-free diffraction intensities, which were further refined. The R_1 values are defined as $R_1 = \Sigma||F_0| - |F_c||/\Sigma|F_0|$ and $wR_2 = \{\Sigma[w(F_0^2 - F_c^2)^2]/\Sigma[w(F_0^2)^2]\}^{1/2}$. Final refinement data are listed in Table 1.

Luminescence Sensing Experiment. Sample of Tb(**1**) was ground and dispersed into ethanol solvent to produce a suspension (1 mg mL^{-1}) by ultrasound method. Then, the chemicals such as 1-HP or urine constituents were added to the suspension. Luminescence spectra of the resulting suspension were collected after being sonicated for 5 min.

RESULTS AND DISCUSSION

Crystal Structures. The reaction of $Ln(NO_3)_3$ (Ln = Tb(**1**), Eu(**2**), and Gd(**3**)) and H_4−BODSDC in CH_3CN/H_2O solvent yielded compound $\{(H_3O)[Ln(BODSDC)(H_2O)_2]\}_n$. The $Tb_{0.93}Eu_{0.07}$-BODSDC compound was obtained similarly to Tb(**1**), except for utilizing $Tb(NO_3)_3$/$Eu(NO_3)_3$ (0.95/0.05 (mole ratio)). These compounds are isomorphous, as revealed by single-crystal X-ray diffraction analyses (Table 1). Tb(**1**) was selected for describing their structures in detail. Tb(**1**) crystallizes in a monoclinic space group *P2/c* and has a 3D framework with 1D channels. The asymmetric unit of Tb(**1**) contains two Tb(III) ions with the occupation of 0.5, one BODSDC^{4-}, and two coordinated water molecules. The two Tb(III) ions are located at two-fold axes exhibiting similar coordination geometry. Each Tb(III) ion is coordinated by four carboxylate oxygens and two sulfonate oxygens from four BODSDC^{4-} ligands and two water oxygens (Figure S1 in the Supporting Information). The Tb−O bond lengths vary from 2.321(2) to 2.4561(19) Å. The BODSDC^{4-} ligand bridges four Tb(III) ions using its four unidentate carboxylate oxygens and two unidentate sulfonate oxygens with the remaining four sulfonate O atoms uncoordinated (Figure S2). The carboxylate groups of the BODSDC^{4-} ligands bridge the Tb(III) ions to give a 1D chain extending along the *c* axis with the closest Tb···Tb separation of 4.6535(1) Å within the 1D chains (Figure S3). Each 1D chain is linked by four neighboring 1D chains through the BODSDC^{4-} ligands. The 1D chains are interconnected with the neighboring 1D chains through the bridging BODSDC^{4-} ligands to give a 3D framework (Figure 1). Because of the semirigid character

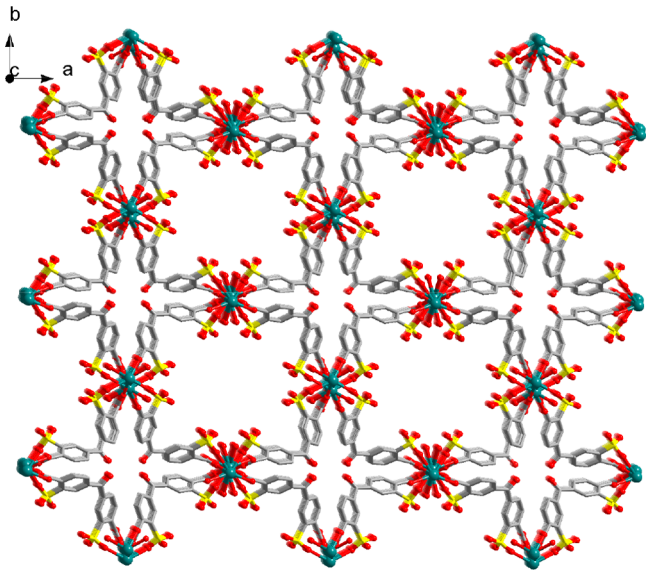

Figure 1. 3D framework of Tb(**1**) showing the sulfonate oxygen-decorated 1D channels.

DOI: 10.1021/acs.inorgchem.8b00865
Inorg. Chem. 2018, 57, 7805−7814

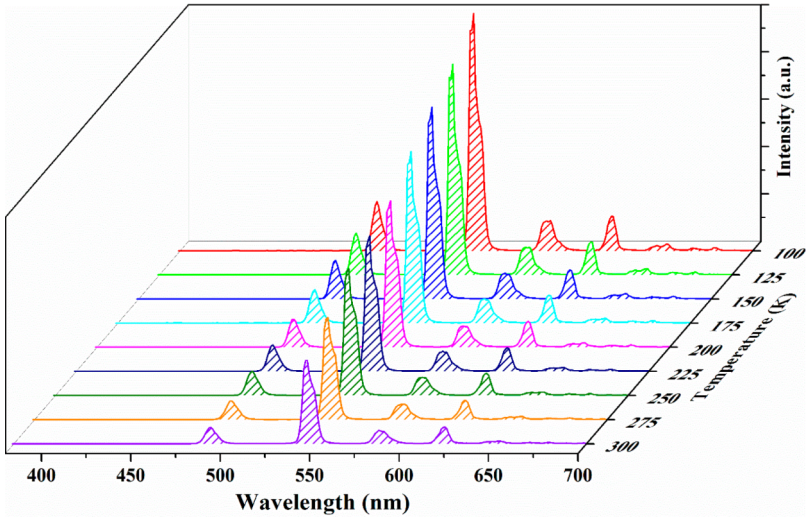

Figure 2. Temperature-dependent emission spectra of Tb(**1**) (λ_{ex} = 368 nm).

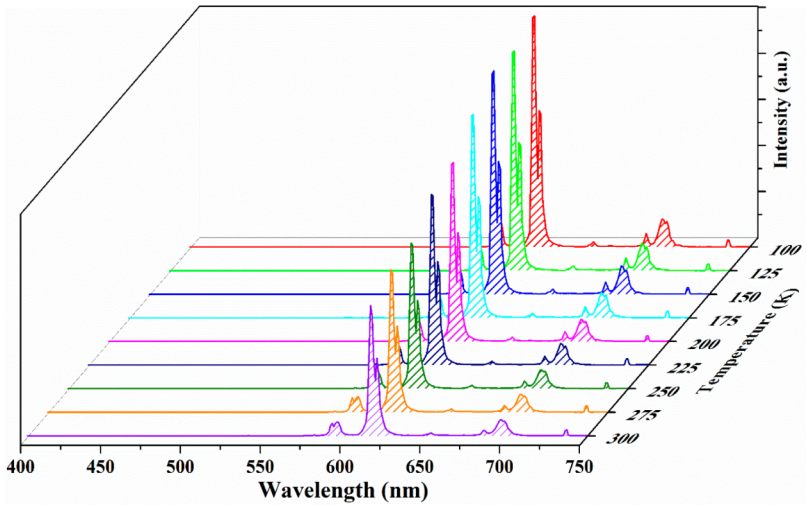

Figure 3. Temperature-dependent mission spectra of Eu(**2**) (λ_{ex} = 368 nm).

and the nonlinear geometry of the $BODSDC^{4-}$ ligand, the 3D framework contains two types of 1D channels extending along the *c* axis. The small 1D channel with the star-like aperture features the carbonyl oxygens pointing to the channels with the closest O···O distance of 4.099 Å (Figure 1). The large square channel has the aperture dimensions of 9.6 × 11.1 $Å^2$ (based on the sulfonate oxygens) with the uncoordinated sulfonate oxygens and water molecules protruding into the channels. The 3D framework of [Tb(BODSDC)$(H_2O)_2$] is an anionic framework that can be charge-balanced by extra-framework hydronium ions (H_3O^+). The disordered guest solvents occupy the voids of the 1D channels. The result of the TGA showed that the solvent molecules were removed between 40 and 130 °C and the collapse of the framework occurred above 400 °C (Figure S4).

Temperature-Dependent Luminescence Properties. The excitation and emission spectra of Tb(**1**) and Eu(**2**) were examined at room temperature in the solid state. Excited at 368 nm, Tb(**1**) exhibits a strong and characteristic Tb(III) emission (Figure S5). The excitation spectrum of Tb(**1**) exhibits an excitation band between 260 and 410 nm, which can be originated from the π transition for the $BODSDC^{4-}$ ligand. In the excitation spectrum, no observable intra-4f peaks from 300 to 450 nm suggests that the Tb(III) ions are completely excited through an effective sensitized process associated with the organic sensitizer. The five characteristic peaks of Tb(III) appear at 489, 544, 584, 622, and 652 nm, which can be assigned to $^5D_4 \rightarrow {}^7F_J$ (J = 6, 5, 4, 3, 2) transitions. The intensity of $^5D_4 \rightarrow {}^7F_5$ transition is more intense than those of other peaks, resulting in a strong green output for the material. Eu(**2**) exhibits a typical radiation emission of the $^5D_0$ excited state of Eu(III) ion when excited at 368 nm (Figure S6). Although the intensities are weak, the sharp intra-$4f^6$ transitions ($^7F_0 \rightarrow {}^5L_6$ (395 nm) and $^7F_0 \rightarrow {}^5D_2$ (464 nm)) for the Eu(III) center are observed in the excitation spectrum. The presence of intra-$4f^6$ lines indicates that the Eu(III) ions are mainly excited by the "'antenna effect"' rather than by direct excitation of the Eu(III) ion. The emission bands appearing at 593, 616, 653, 697, and 736 nm are $^5D_0 \rightarrow {}^7F_J$ (J = 1, 2, 3, 4, and 5) transitions. The quantum yields of Tb(**1**) and Eu(**2**) are determined to be 15.3 and 14.8%, respectively. Such high quantum yields suggest that the lanthanide compounds are excellent candidates for fluorescent probes. As expected, $Tb_{0.93}Eu_{0.07}$-BODSDC simultaneously shows the characteristic Tb(III) and Eu(III) emissions (Figure S7). Such a phenomenon implies that the energy transfer from

DOI: 10.1021/acs.inorgchem.8b00865
Inorg. Chem. 2018, 57, 7805−7814

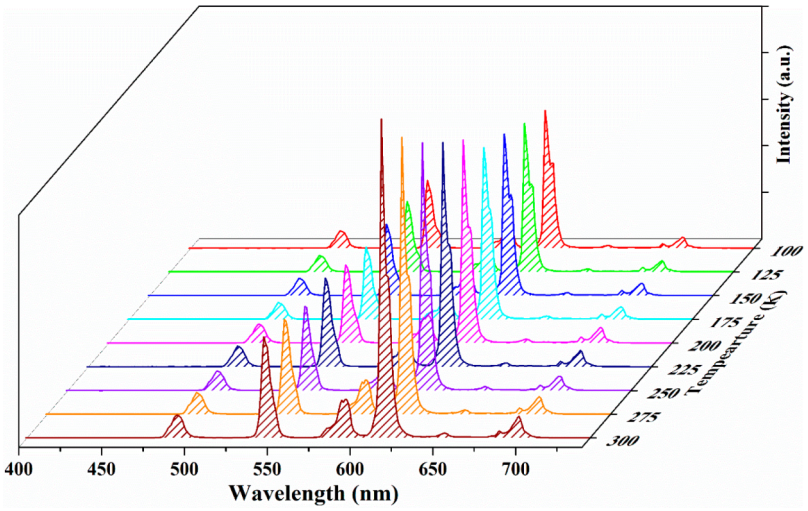

Figure 4. Temperature-dependent emission spectra of $Tb_{0.93}Eu_{0.07}$-BODSDC (λ_{ex} = 368 nm).

the organic ligand to the Tb(III) and Eu(III) ions is efficient. Although the content of the Eu(III) is much lower than that of the Tb(III) in $Tb_{0.93}Eu_{0.07}$-BODSDC, the intensity at 616 nm for Eu(III) is more intense than that of 544 nm for Tb(III) (Figure S7). Thus the present Tb/Eu ratio is the best sample to be examined for its temperature-dependent luminescence spectrum.

The temperature-dependent emission spectra of Tb(**1**) and Eu(**2**) from 100 to 300 K were studied in detail. As depicted in Figures 2 and 3, the intensity of the Tb(III) and Eu(III) emissions decrease with temperature increasing, which is caused by the thermal activation of nonradiative decay pathways.[17] The emission intensity and lifetime of the $^5D_0 \rightarrow {}^7F_2$ peak for Eu(III) in Eu(**2**) decrease more slowly than those of the $^5D_4 \rightarrow {}^7F_5$ peak for Tb(III) in Tb(**1**) as temperature increases (Figure S8 and S9), which results from the different energy gaps between the ligand's triplet excited state and the lanthanide ions' emitting levels. The energy of the triplet excited state T_1 of H_4BODSDC can be estimated from the emission spectrum of Gd(**3**) at 77 K, which gives the value of 27 548 cm^{-1} (Figure S10). The energy gap between T_1 and $^5D_0$ emitting level of Eu(III) (17 267 cm^{-1})[18] is significantly larger than that between the T_1 and $^5D_4$ emitting level of Tb(III) (20 453 cm^{-1}),[19] which prohibits the thermally driven depopulation.[20]

The $Tb_{0.93}Eu_{0.07}$-BODSDC with two kinds of emitting centers is expected to be a ratiometric luminescent sensor without any additional calibration of emission intensity. The temperature-dependent emission spectra of $Tb_{0.93}Eu_{0.07}$-BODSDC show that the intensity of $^5D_0 \rightarrow {}^7F_2$ emission band (616 nm) for Eu(III) increases significantly, whereas the $^5D_4 \rightarrow {}^7F_5$ emission band (544 nm) for Tb(III) decreases slowly, as temperature increases (Figures 4 and 5). The intensity of the $^5D_0 \rightarrow {}^7F_2$ emission band (Eu(III)) at 300 K is about 2.3 times stronger than that at 100 K, whereas the intensity of the $^5D_4 \rightarrow {}^7F_5$ emission band (Tb(III)) at 300 K is 0.65 times weaker than that of 100 K. The dramatic changes of intensity for Tb(III)- and Eu(III)-originated emissions in opposite directions indicate that the present $Tb_{0.93}Eu_{0.07}$-BODSDC material is expected to be a promising ratiometric luminescent thermometer. As depicted in the inset of Figure 5, the emission intensity ratio (Δ) of the $^5D_4 \rightarrow {}^7F_5$ emission band (Tb(III), 544 nm) to the $^5D_0 \rightarrow {}^7F_2$ emission band

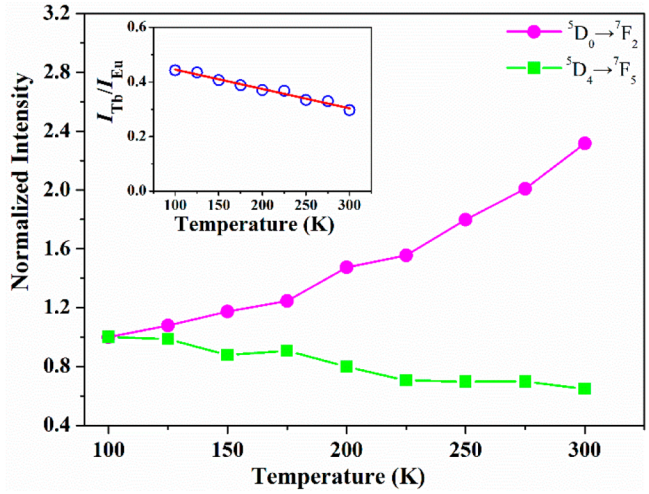

Figure 5. Temperature-dependent integrated intensities of $^5D_4 \rightarrow {}^7F_5$ (536−556 nm) and $^5D_0 \rightarrow {}^7F_2$ (604−633 nm) emission bands of $Tb_{0.93}Eu_{0.07}$-BODSDC. Inset: Temperature dependence of the integrated intensity ratio of $^5D_4 \rightarrow {}^7F_5$ emission band to $^5D_0 \rightarrow {}^7F_2$ emission band for $Tb_{0.93}Eu_{0.07}$-BODSDC. (The solid line is fitted with a linear equation.)

(Eu(III), 616 nm) ($\Delta = I_{Tb}/I_{Eu}$) decreases linearly with temperature (T) from 100 to 300 K. The fitting of linear equation, $\Delta = 0.51678 - 0.00071T$, gives the correlation coefficient R^2 of 0.97843, indicating that the $Tb_{0.93}Eu_{0.07}$-BODSDC material is a luminescent thermometer between 100 and 300 K. The relative thermal sensitivity S_r with the advantage of being independent of the nature of the thermometers, which is defined as $|\partial\Delta/\partial T|/\Delta$,[21] is commonly for evaluation of the thermometer performance. Because the Δ value is dependent on the temperature T, the S_r values vary with T. The maximum value (S_m) of S_r within the test temperature is proposed for comparing the performance of the distinct Ln-MOF thermometers.[22] According to the linear equation, the relative thermal sensitivity S_m for $Tb_{0.93}Eu_{0.07}$-BODSDC is 0.23% K^{-1} at 300 K, which is comparable to those for the $Tb_{0.9989}Eu_{0.0011}$-DMBDC compound[23] and $Tb_{0.99}Eu_{0.01}(bdc)_{1.5}(H_2O)_2$[24] but larger than that of $Tb_{0.9}Eu_{0.1}$-L (L = 1,3-bis(4-carboxyphenyl)imidazolium).[25]

DOI: 10.1021/acs.inorgchem.8b00865
Inorg. Chem. 2018, 57, 7805−7814

These results indicate that the $Tb_{0.93}Eu_{0.07}$-BODSDC is a useful ratiometric luminescent thermometer.

Because the emission color of $Tb_{0.93}Eu_{0.07}$-BODSDC is synergistically originated from Eu(III) and Tb(III) dual emission, the emission color will change with the intensity ratio of Eu(III) and Tb(III) emission at different temperature. The chromaticity coordinates can be calculated from the emission spectra of $Tb_{0.93}Eu_{0.07}$-BODSDC.[26] The result of the calculations shows that the chromaticity coordinates change from (0.5233, 0.4404) at 100 K to (0.5430, 0.4289) at 300 K (Figure 6). As a result, the emissive light colors of $Tb_{0.93}Eu_{0.07}$-BODSDC shift from the yellow region to the red region when the temperature ranges from 100 to 300 K.

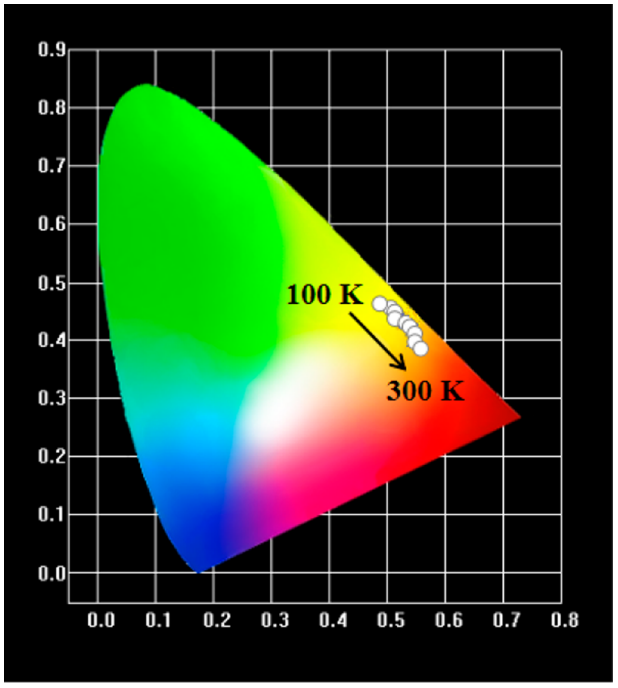

Figure 6. CIE chromaticity diagram for $Tb_{0.93}Eu_{0.07}$-BODSDC.

To understand the mechanism of temperature-dependent emission of $Tb_{0.93}Eu_{0.07}$-BODSDC, the lifetimes of the $^5D_0$ emitting level of Eu(III) and $^5D_4$ emitting level of Tb(III) for $Tb_{0.93}Eu_{0.07}$-BODSDC at different temperatures were monitored at 616 and 544 nm, respectively (Figure S11). The $^5D_4$ lifetime of Tb(III) in $Tb_{0.93}Eu_{0.07}$-BODSDC is much lower than that in Tb(**1**) at the same temperature, whereas the $Tb_{0.93}Eu_{0.07}$-BODSDC possesses a longer $^5D_0$ lifetime of Eu(III) than that in Eu(**2**) at the same temperature. The $^5D_0$ lifetime in $Tb_{0.93}Eu_{0.07}$-BODSDC increased by ~9.8% as the temperature was increased from 100 to 300 K. Such results suggested that energy from the Tb(III) to Eu(III) ions occurred. Thus the temperature-dependent luminescence behavior of $Tb_{0.93}Eu_{0.07}$-BODSDC can be assigned to the probability of temperature-dependent energy transfer from the Tb(III) to Eu(III) ions. Commonly, the energy-transfer efficiency (η) is calculated from the donor lifetime of Tb(III) with (τ) and without (τ_0) the Eu(III) acceptor by the equation $\eta = 1 - \tau/\tau_0$.[27] The calculated η versus T plot for $Tb_{0.93}Eu_{0.07}$-BODSDC is depicted in Figure S12. The energy-transfer efficiency η from Tb(III) to Eu(III) is enhanced upon the temperature increasing from 100 to 300 K, which is mainly controlled by the phonon-assisted Förster transfer mechanism.[28] As a result, the emission intensity of Eu(III) is enhanced with temperature increase based on the cost of the quenching of Tb(III) emission.

Luminescence Sensing of 1-HP. As is well known, Tb(III) compounds can display characteristic green-color emission, which has potential as a luminescence sensor. 1-HP is a metabolite of polycyclic aromatic hydrocarbon (PAHs) carcinogens in human urine. Because the 1-HP is nearly insoluble in the aqueous solution, the ethanol solvent is used for the luminescence experiments. To evaluate the sensing properties of Tb(**1**) toward 1-HP, the 1-HP was added to the suspension of Tb(**1**) in ethanol. As shown in Figure 7, the

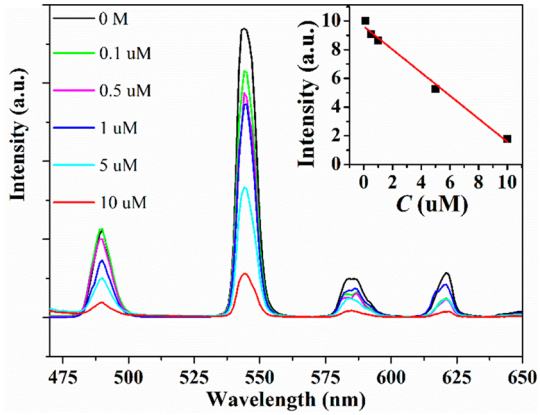

Figure 7. Emission spectra of Tb(**1**) suspensions in the presence of 1-HP. Inset: The luminescence intensity of $^5D_4 \rightarrow {}^7F_5$ transition (I_{544}) versus 1-HP concentration (0.1−10 uM) for Tb(**1**) (λ_{ex} = 368 nm).

addition of 1-HP to the suspension of Tb(**1**) (Tb(**1**) concentration: 1 mg/mL) leads to weakening Tb(**1**) emission. The emission intensity of Tb(III) at 544 nm gradually decreases as 1-HP concentration increases. When the content of 1-HP is 10 uM, the fluorescence quenching efficiency is sharply reduced (84.8%) (Figure 7), indicating the high sensitivity of Tb(**1**) for 1-HP detection. The dependence of emission intensity at 544 nm (I_{544}) versus the 1-HP concentration (C) is plotted in the inset of Figure 7. A good linear correlation between I_{544} and C (I_{544} = 9.62198 − 0.0832C) is obtained within the 1-HP concentration from 0.1 to 10 uM with a correlation coefficient (R^2) of 0.98833. Such results imply that Tb(**1**) is an excellent fluorescent probe for quantitative analysis of 1-HP. On the basis of the 3σ/slope IUPAC criteria, the limit of detection (LOD) is 0.09 μg L^{-1}, which is lower than the benchmark value (1-HP: 1.0 μg L^{-1}) in urine recommended by the American Conference of Governmental Industrial Hygienists.[29] Thus Tb(**1**) has a high sensitivity for detecting of 1-HP.

To investigate the urine constituents on the detection of 1-HP, the main urine constituents of creatinine, creatine, glucose, urea, uric acid, hippuric acid, K^+, Na^+, NH_4^+, and Cl^- were added to the Tb(**1**) suspensions. As illustrated in Figure S13, the characteristic Tb(III) emissions were observed for all urine constituent-incorporated Tb(**1**) (concentration of urine constituent: 1 mM). The intensities of the dominant emission (544 nm) of Tb(**1**) suspensions in the presence of urine constituents are depicted in Figure 8. As demonstrated in Figures S13 and Figure 8, no significant change was detected in the Tb(III) emission when other urine constituents were introduced to the system. Moreover, to explore the influence of

DOI: 10.1021/acs.inorgchem.8b00865
Inorg. Chem. 2018, 57, 7805−7814

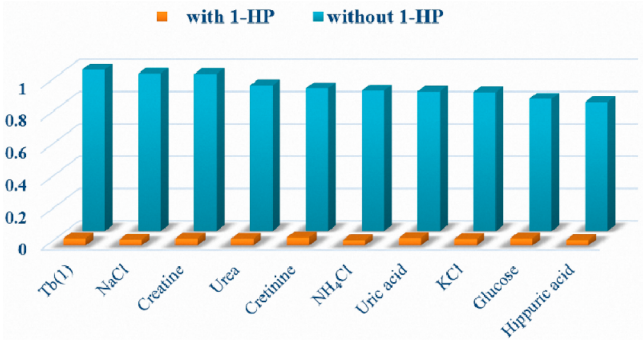

Figure 8. Emission intensity at 544 nm of Tb(**1**) suspensions with urine constituents (concentration: 1 mM) in the absence and presence of 1-HP (concentration: 0.1 mM) (λ_{ex} = 368 nm).

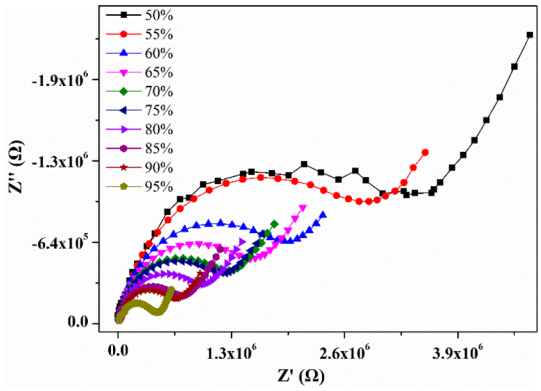

Figure 9. Nyquist plots for the pellet of Tb(**1**) at 25 °C and various RH.

other urine constituents on 1-HP sensing, the competition experiments were performed. Because of the large fluorescence quenching effect of 1-HP, the used concentration for 1-HP and other urine constituents was 0.1 and 1 mM, respectively, in the competition experiments. As depicted in Figure 8, the quenching effect of 1-HP is not affected by other urine constituents. The present results demonstrate that the 1-HP can be solely sensed by Tb(**1**) without interference from other urinary species. Therefore, Tb(**1**) can potentially serve as a highly selective probe for 1-HP with a high antijamming capability.

Finally, the mechanism for detecting 1-HP by Tb(**1**) with luminescence quenching was studied. As shown in Figure S14, the PXRD pattern of 1-HP-incorporated Tb(**1**) sample is very close to the pristine one, indicating that the framework remains intact after the addition of 1-HP. As illustrated in Figure 1, the Tb(III) ions in 3D structure are well shielded by the carboxylate and sulfonate groups as well as the coordinated water molecules. This indicates that the fluorescence quenching through a direct interaction between the emission centers of Tb(III) and the large skeleton of 1-HP is not feasible. Moreover, the UV−vis absorption spectrum of 1-HP does not overlap with the emission band of the H_4BODSDC ligand (Figure S15). Thus the fluorescence resonance energy transfer[30] from the BODSDC^{4-} ligand to 1-HP is impossible for Tb(**1**). Because the 1D channels' surfaces are full of sulfonate oxygens, when the 1-HP was added to the Tb(**1**), the 1-HP diffused into the 1D channels and formed the hydrogen bonds with the sulfonate oxygens through its hydroxyl group. Such interactions will perturb the electronic structure of the BODSDC^{4-} ligand and thus block the energy transfer from BODSDC^{4-} ligands to the Tb(III) centers, leading to luminescence quenching.

Proton Conduction. The organic polymers containing the sulfonate groups are an important type of solid-state proton-conducting materials.[31] Very recently, the MOFs with the sulfonated ligand were found to show high conductivity.[32] As depicted in Figure 1, the 1D hydrophilic channels were lined with sulfonate oxygens and coordinated water molecules, which are the potential binding sites for protons. Such a structural feature indicates that these compounds are the candidates for proton-conductive materials. Because all compounds have the same hydrophilic channels, the proton conductivity of Tb(**1**) was therefore representatively assessed by the AC impedance method. Figure 9 shows the Nyquist plots for Tb(**1**) at 25 °C under different relative humidity (RH). The Nyquist plots feature a semicircle and an inclined tail in the high-frequency and low-frequency components, respectively, which is a fingerprint of proton conducting materials. The proton conductivity (σ) of Tb(**1**) at 25 °C is 1.17×10^{-6} and 2.16×10^{-5} S cm^{-1} under 50 and 95% RH, respectively, which indicates that the conductivity is highly humidity-dependent. The proton conductivity is enhanced with RH increase. The conductivity at 95% RH is comparable to those of other lanthanide MOFs such as the 3D Sm-compound (4.69×10^{-5} S cm^{-1} under 30 °C and 98% RH),[33] the 3D Gd-compound (6.3×10^{-5} S cm^{-1} under 25 °C and 97% RH),[34] and layered La compound (4.24×10^{-5} S cm^{-1} at 25 °C and 95% RH).[35] The highly humidity-dependent conductivity is corroborated by the Nyquist plots (Figure 9), which show a noticeable decrease in the semicircles with increasing humidity. With increasing humidity, the framework adsorbed more water molecules, which are hydrogen-bonded with the sulfonate oxygens and coordinated water in the 1D channels, resulting in this high proton conductivity.

To get more insight into the proton conduction, the conductivities of Tb(**1**) under 95% RH in the temperature range from 25 to 85 °C were measured (Figure S16). The size of the semicircles was reduced as the temperature was raised, as shown in the Nyquist plots. The considerable increase in the conductivity with temperature increasing was observed. The σ values increased from 2.16×10^{-5} S cm^{-1} at 25 °C to 6.57×10^{-4} S cm^{-1} at 85 °C under 95% RH, which is comparable to that of the Gd-oxalate compound (4.7×10^{-4} S cm^{-1} at 95% RH and 80 °C).[36] The thermal activation of water molecules in the higher temperature accounts for the enhancement of the conductivity. The activation energy E_a for proton conduction can be extracted from the temperature dependence data. The Arrhenius law was used to fit the conductivities in the form of $\ln(\sigma T)$ versus T^{-1}, giving the E_a of 0.541 eV (Figure 10). Such a value indicates that a vehicle mechanism dominates the proton transport in Tb(**1**).[37] The solvate water molecules gather together in the hydrophilic channels and move as solvated H_3O^+, leading to a vehicle-type proton transfer.

Finally, no distinct change is observed in the humidity-dependent proton conductivities obtained by repeatedly decreasing and increasing the humidity from 50 to 95% at 85 °C (Figure 11). The reproducible conduction data indicate that Tb(**1**) is stable under impedance measurements, further corroborated by the PXRD pattern (Figure S14), which showed that the integrity of the sample was maintained after impedance measurements. Additionally, Tb(**1**) shows a steady

DOI: 10.1021/acs.inorgchem.8b00865
Inorg. Chem. 2018, 57, 7805−7814

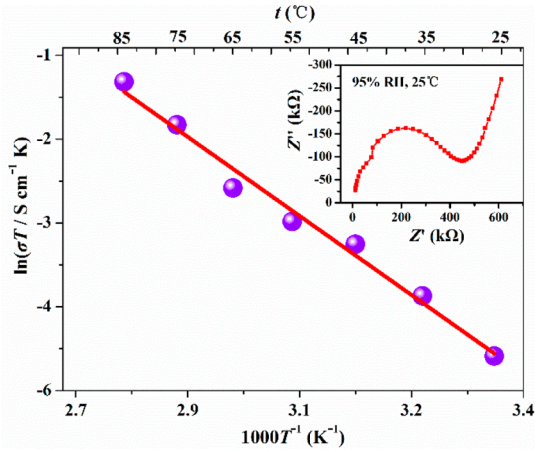

Figure 10. Arrhenius plots for Tb(**1**) under 95% RH. The red solid line represents the best fit of the data. The data were collected at 10 °C intervals from 25 to 85 °C. Each data point is obtained by three independent tests. Inset: Nyquist plot for Tb(**1**) at 25 °C and 95% RH.

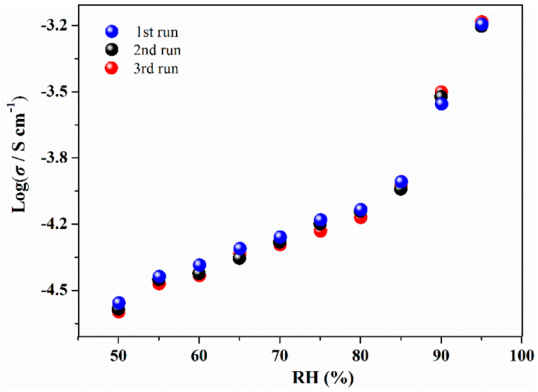

Figure 11. log(σ) versus RH plots of Tb(**1**) at 85 °C with three cycles.

increase in conductivity when the RH is increased from 50 to 85%, whereas the conductivity experiences a much more abrupt increase as the RH increases from 85 to 95% (Figure 11).

CONCLUSIONS

A novel bifunctional benzophenone-3,3′-disulfonyl-4,4′-dicarboxylic acid (H_4–BODSDC) ligand and the lanthanide compounds based on the H_4–BODSDC ligand displaying 3D frameworks have been synthesized and characterized. The lanthanide ions are efficiently sensitized by the organic ligand to give the characteristic luminescence of Tb(III) and Eu(III) ions in Tb(**1**) and Eu(**2**), respectively. The binary $Tb_{0.93}Eu_{0.07}$-BODSDC behaves as a ratiometric fluorescence thermometer over a wide temperature range. In addition, the Tb(**1**) was developed as a fluorescent sensor for 1-HP. Finally, the high-density hydrophilic sulfonate groups are arranged on the 1D channels and enrich the solvate water molecules, resulting in a high proton conductivity of Tb(**1**). The present work provides an excellent example for the design of multifunctional MOF materials based on the organic ligands with different functional groups.

ASSOCIATED CONTENT

Supporting Information

The Supporting Information is available free of charge on the ACS Publications website at DOI: 10.1021/acs.inorgchem.8b00865.

X-ray structure data in CIF format, PXRD patterns, TG curves, luminescence plots, and proton conductivity data. (PDF)

Accession Codes

CCDC 1831920–1831922 contain the supplementary crystallographic data for this paper. These data can be obtained free of charge via www.ccdc.cam.ac.uk/data_request/cif, or by emailing data_request@ccdc.cam.ac.uk, or by contacting The Cambridge Crystallographic Data Centre, 12 Union Road, Cambridge CB2 1EZ, UK; fax: +44 1223 336033.

AUTHOR INFORMATION

Corresponding Authors

*Y.-L.W.: E-mail: ylwang@jxnu.edu.cn. Fax: +86-791-88336372.

*Q.-Y.L.: E-mail: qyliuchem@jxnu.edu.cn.

ORCID

Yu-Ling Wang: 0000-0002-0839-699X

Qing-Yan Liu: 0000-0003-1991-792X

Notes

The authors declare no competing financial interest.

ACKNOWLEDGMENTS

We acknowledge the National Natural Science Foundation of China (nos. 21661014, 21561015, and 21361011) and the key project of Natural Science Foundation of Jiangxi Province (20171ACB20008).

REFERENCES

(1) (a) Long, J. R.; Yaghi, O. M. The pervasive chemistry of metal–organic frameworks. *Chem. Soc. Rev.* **2009**, *38*, 1213–1214. (b) Zhou, H.-C.; Long, J. R.; Yaghi, O. M. Introduction to Metal–Organic frameworks. *Chem. Rev.* **2012**, *112*, 673–674. (c) Zhou, H.-C.; Kitagawa, S. Metal–Organic Frameworks (MOFs). *Chem. Soc. Rev.* **2014**, *43*, 5415–5418.

(2) (a) Li, J.-R.; Sculley, J.; Zhou, H.-C. Metal–Organic Frameworks for Separations. *Chem. Rev.* **2012**, *112*, 869–932. (b) Liu, J.; Chen, L.; Cui, H.; Zhang, J.; Zhang, L.; Su, C.-Y. Applications of metal–organic frameworks in heterogeneous supramolecular catalysis. *Chem. Soc. Rev.* **2014**, *43*, 6011–6061. (c) Lee, J.; Farha, O. K.; Roberts, J.; Scheidt, K. A.; Nguyen, S. T.; Hupp, J. T. Metal–organic framework materials as catalysts. *Chem. Soc. Rev.* **2009**, *38*, 1450–1459. (d) Yoon, M.; Suh, K.; Natarajan, S.; Kim, K. Proton Conduction in Metal–Organic Frameworks and Related Modularly Built Porous Solids. *Angew. Chem., Int. Ed.* **2013**, *52*, 2688–2700.

(3) (a) Rocha, J.; Carlos, L. D.; Paz, A. A.; Ananias, D. Luminescent multifunctional lanthanides-based metal–organic frameworks. *Chem. Soc. Rev.* **2011**, *40*, 926–940. (b) Cui, Y.; Yue, Y.; Qian, G.; Chen, B. Luminescent Functional Metal–Organic Frameworks. *Chem. Rev.* **2012**, *112*, 1126–1162. (c) Sorace, L.; Benelli, C.; Gatteschi, D. Lanthanides in molecular magnetism: old tools in a new field. *Chem. Soc. Rev.* **2011**, *40*, 3092–3104.

(4) (a) Hao, J.-N.; Yan, B. Ag^+-sensitized in Ln^{3+} post-functionalized lanthanide luminescence metal–organic frameworks and Ag^+ sensing. *J. Mater. Chem. A* **2015**, *3*, 4788–4792. (b) Zhou, L.-J.; Deng, W.-H.; Wang, Y.-L.; Xu, G.; Yin, S.-G.; Liu, Q.-Y. Lanthanide–Potassium Biphenyl-3,3′-disulfonyl –4,4′-dicarboxylate Frameworks: Gas Sorption, Proton Conductivity, and Luminescent Sensing of Metal Ions. *Inorg. Chem.* **2016**, *55*, 6271–6277. (c) Hao, J.-N.; Yan, B. A. water-

DOI: 10.1021/acs.inorgchem.8b00865
Inorg. Chem. 2018, 57, 7805–7814

stable lanthanide-functionalized MOF as a highly selective and sensitive fluorescent probe for Cd^{2+}. *Chem. Commun.* **2015**, *51*, 7737−7740. (d) Chen, B. L.; Wang, L. B.; Zapata, F.; Qian, G. D.; Lobkovsky, E. B. A Luminescent Microporous Metal−Organic Framework for the Recognition and Sensing of Anions. *J. Am. Chem. Soc.* **2008**, *130*, 6718−6719. (e) Sun, N.-N.; Yan, B. Rapid and facile ratiometric detection of CO_3^{2-}based on heterobimetallic metal−organic frameworks (Eu/Pt−MOFs). *Dyes Pigm.* **2017**, *142*, 1−7.

(5) (a) Li, Y.; Zhang, S. S.; Song, D. T. A Luminescent Metal−Organic Framework as a Turn−On Sensor for DMF Vapor. *Angew. Chem.* **2013**, *125*, 738−741. (b) Wang, X. Q.; Zhang, L. L.; Yang, J.; Liu, F. L.; Dai, F. N.; Wang, R. M.; Sun, D. F. Lanthanide metal−organic frameworks containing a novel flexible ligand for luminescence sensing of small organic molecules and selective adsorption. *J. Mater. Chem. A* **2015**, *3*, 12777−12785. (c) Peng, J. J.; Teoh, C. L.; Zeng, X.; Samanta, A.; Wang, L.; Xu, W.; Su, D. D.; Yuan, L.; Liu, X. G.; Chang, Y.-T. Development of a Highly Selective, Sensitive, and Fast Response Upconversion Luminescent Platform for Hydrogen Sulfide Detection. *Adv. Funct. Mater.* **2016**, *26*, 191−199. (d) Liu, X.-J.; Zhang, Y.-H.; Chang, Z.; Li, A.-L.; Tian, D.; Yao, Z.-Q.; Jia, Y.-Y.; Bu, X. -H. A. Water-Stable Metal−Organic Framework with a Double-Helical Structure for Fluorescent Sensing. *Inorg. Chem.* **2016**, *55*, 7326−7328. (e) He, R.; Wang, Y.-L.; Ma, H.-F.; Yin, S.-G.; Liu, Q.-Y. Eu^{3+}-functionalized metal−organic framework composite as ratiometric fluorescent sensor for highly selective detecting urinary 1-hydroxypyrene. *Dyes Pigm.* **2018**, *151*, 342−347.

(6) (a) Rao, X. T.; Song, T.; Gao, J. K.; Cui, Y. J.; Yang, Y.; Wu, C. D.; Chen, B. L.; Qian, G. D. A Highly Sensitive Mixed Lanthanide Metal−Organic Framework Self-Calibrated Luminescent Thermometer. *J. Am. Chem. Soc.* **2013**, *135*, 15559−15564. (b) Zhou, Y.; Yan, B.; Lei, F. Postsynthetic lanthanide functionalization of nanosized metal−organic frameworks for highly sensitive ratiometric luminescent thermometry. *Chem. Commun.* **2014**, *50*, 15235−15238. (c) Yang, Y.; Chen, L.; Jiang, F. L.; Yu, M. X.; Wan, X. Y.; Zhang, B.; Hong, M. C. A family of doped lanthanide metal−organic frameworks for wide-range temperature sensing and tunable white light emission. *J. Mater. Chem. C* **2017**, *5*, 1981−1989.

(7) (a) Li, Y.-J.; Wang, Y.-L.; Liu, Q.-Y. The Highly Connected MOFs Constructed from Nonanuclear and Trinuclear Lanthanide-Carboxylate Clusters: Selective Gas Adsorption and Luminescent pH Sensing. *Inorg. Chem.* **2017**, *56*, 2159−2164. (b) Lu, Y.; Yan, B. A ratiometric fluorescent pH sensor based on nanoscale metal−organic frameworks (MOFs) modified by europium(III) complexes. *Chem. Commun.* **2014**, *50*, 13323−13326.

(8) Bünzli, J. -C. G. Benefiting from the Unique Properties of Lanthanide Ions. *Acc. Chem. Res.* **2006**, *39*, 53−61.

(9) (a) Deria, P.; Chung, Y. G.; Snurr, R. Q.; Hupp, J. T.; Farha, O. K. Water stabilization of Zr_6-based metal−organic frameworksvia solvent-assisted ligand incorporation. *Chem. Sci.* **2015**, *6*, 5172−5176. (b) Taylor, J. M.; Komatsu, T.; Dekura, S.; Otsubo, K.; Takata, M.; Kitagawa, H. The Role of a Three Dimensionally Ordered Defect Sublattice on the Acidity of a Sulfonated Metal−Organic Framework. *J. Am. Chem. Soc.* **2015**, *137*, 11498−11506. (c) Yang, F.; Huang, H.; Wang, X.; Li, F.; Gong, Y.; Zhong, C.; Li, J.-R. Proton Conductivities in Functionalized UiO-66: Tuned Properties, Thermogravimetry Mass, and Molecular Simulation Analyses. *Cryst. Growth Des.* **2015**, *15*, 5827−5833. (d) Xue, D.-X.; Cairns, A. J.; Belmabkhout, Y.; Wojtas, L.; Liu, Y.; Alkordi, M. H.; Eddaoudi, M. Tunable Rare-Earth fcu-MOFs: A Platform for Systematic Enhancement of CO_2 Adsorption Energetics and Uptake. *J. Am. Chem. Soc.* **2013**, *135*, 7660−7667. (e) Zhang, Y.-B.; Furukawa, H.; Ko, N.; Nie, W.; Park, H. J.; Okajima, S.; Cordova, K. E.; Deng, H.; Kim, J.; Yaghi, O. M. Introduction of Functionality, Selection of Topology, and Enhancement of Gas Adsorption in Multivariate Metal−Organic Framework-177. *J. Am. Chem. Soc.* **2015**, *137*, 2641−2650.

(10) (a) Côté, A. P.; Shimizu, G. K. H. The supramolecular chemistry of the sulfonate group in extended solids. *Coord. Chem. Rev.* **2003**, *245*, 49−64. (b) Shimizu, G. K. H.; Vaidhyanathan, R.; Taylor, J. M. Phosphonate and sulfonate metal organic frameworks. *Chem. Soc. Rev.* **2009**, *38*, 1430−1449. (c) Sun, D.; Liu, F.-J.; Hao, H.-J.; Li, Y.-H.; Zhang, N.; Huang, R.-B.; Zheng, L.-S. A novel arenedisulfonate-templated 1D silver ladder constructed from 4-aminobenzonitrile ligand. *CrystEngComm* **2011**, *13*, 5661−5665. (d) Meng, X.; Song, S.-Y.; Song, X.-Z.; Zhu, M.; Zhao, S. - N.; Wu, L.-L.; Zhang, H.-J. A tetranuclear copper cluster-based MOF with sulfonate−carboxylate ligands exhibiting high proton conduction properties. *Chem. Commun.* **2015**, *51*, 8150−8152. (e) Dong, X.-Y.; Wang, R.; Li, J.-B.; Zang, S.-Q.; Hou, H.-W.; Mak, T. C. W. A tetranuclear $Cu_4(\mu_3\text{-}OH)_2$-based metal−organic framework (MOF) with sulfonate−carboxylate ligands for proton conduction. *Chem. Commun.* **2013**, *49*, 10590−10592.

(11) (a) Singh, N.; Kaur, N.; Dunn, J.; MacKay, M.; Callan, J. F. A new fluorescent chemosensor for iron(III) based on the β-aminobisulfonate receptor. *Tetrahedron Lett.* **2009**, *50*, 953−956. (b) Neofotistou, E.; Malliakas, C. D.; Trikalitis, P. N. Unprecedented Sulfone−Functionalized Metal−Organic Frameworks and Gas−Sorption Properties. *Chem. - Eur. J.* **2009**, *15*, 4523−4527. (c) Horike, S.; Bureekaew, S.; Kitagawa, S. Coordination pillared-layer type compounds having pore surface functionalization by anionic sulfonategroups. *Chem. Commun.* **2008**, 471−473.

(12) (a) Xiao, B.; Byrne, P. J.; Wheatley, P. S.; Wragg, D. S.; Zhao, X.; Fletcher, A. J.; Thomas, K. M.; Peters, L.; Evans, J. S. O.; Warren, J. E.; Zhou, W.; Morris, R. E. Chemically blockable transformation and ultraselective low-pressure gas adsorption in a non-porous metal organic framework. *Nat. Chem.* **2009**, *1*, 289−294. (b) Horike, S.; Matsuda, R.; Tanaka, D.; Mizuno, M.; Endo, K.; Kitagawa, S. Immobilization of Sodium Ions on the Pore Surface of a Porous Coordination Polymer. *J. Am. Chem. Soc.* **2006**, *128*, 4222−4223. (c) Sun, D. F.; Cao, R.; Sun, Y. Q.; Bi, W. H.; Yuan, D. Q.; Shi, Q.; Li, X. Syntheses and structures of two novel copper complexes constructed from unusual planar tetracopper(II) SBUs. *Chem. Commun.* **2003**, 1528−1529. (d) Miao, X.-H.; Zhu, L.-G. Synthesis, supramolecular structures and catalytic properties of nickel(II) 3-sulfobenzoate complexes with chelating amine ligands. *CrystEngComm* **2009**, *11*, 2500−2509. (e) Liu, Q.-Y.; Wang, W.-F.; Wang, Y.-L.; Shan, Z.-M.; Wang, M.-S.; Tang, J. K. Diversity of Lanthanide(III)−Organic Extended Frameworks with a 4,8-Disulfonyl-2,6-naphthalenedicarboxylic Acid Ligand: Syntheses, Structures, and Magnetic and Luminescent Properties. *Inorg. Chem.* **2012**, *51*, 2381−2392. (f) Liu, Q.-Y.; Li, L.-Q.; Wang, Y.-L.; Yang, E.-L.; Wei, J.-J.; Fu, J.-H. New heterometallic frameworks with flexible sulfonate-carboxylate ligand: syntheses, structures, and properties. *CrystEngComm* **2011**, *13*, 6150−6156.

(13) *CrysAlisPro*; Rigaku Oxford Diffraction: The Woodlands, TX, 2015.

(14) Sheldrick, G. M. SHELXT−Integrated space-group and crystal-structure determination. *Acta Crystallogr., Sect. A: Found. Adv.* **2015**, *A71*, 3−8.

(15) Sheldrick, G. M. Crystal structure efinement with SHELXL. *Acta Crystallogr., Sect. C: Struct. Chem.* **2015**, *71*, 3−8.

(16) Spek, A. L. *PLATON: A Multipurpose Crystallographic Tool*; Utrecht University: Utrecht, The Netherlands, 2001.

(17) (a) Bhaumik, M. L. Quenching and Temperature Dependence of Fluorescence in Rare−Earth Chelates. *J. Chem. Phys.* **1964**, *40*, 3711−3715. (b) Weissman, S. I. Intramolecular Energy Transfer The Fluorescence of Complexes of Europium. *J. Chem. Phys.* **1942**, *10*, 214−217. (c) Peng, H. S.; Stich, M. I. J.; Yu, J. B.; Sun, L.-N.; Fischer, L. H.; Wolfbeis, O. S. Luminescent Europium(III) Nanoparticles for Sensing and Imaging of Temperature in the Physiological Range. *Adv. Mater.* **2010**, *22*, 716−719.

(18) Carnall, W. T.; Fields, P. R.; Rajnak, K. Electronic Energy Levels in the Trivalent Lanthanide Aquo Ions. I. Pr^{3+}, Nd^{3+}, Pm^{3+}, Sm^{3+}, Dy^{3+}, Ho^{3+}, Er^{3+}, and Tm^{3+}. *J. Chem. Phys.* **1968**, *49*, 4450−4455.

(19) Carnall, W. T.; Fields, P. R.; Rajnak, K. Electronic Energy Levels of the Trivalent Lanthanide Aquo Ions. III. Tb^{3+}. *J. Chem. Phys.* **1968**, *49*, 4447−4449.

(20) (a) Carlos, L. D.; Ferreira, R. A. S.; de Zea Bermudez, V.; JulianLopez, B.; Escribano, P. Progress on lanthanide-based organic−

DOI: 10.1021/acs.inorgchem.8b00865
Inorg. Chem. 2018, 57, 7805−7814

inorganic hybrid phosphors. *Chem. Soc. Rev.* **2011**, *40*, 536−549. (b) Brites, C. D. S.; Lima, P. P.; Silva, N. J. O.; Millán, A.; Amaral, V. S.; Palacio, F.; Carlos, L. D. A Luminescent Molecular Thermometer for Long−Term Absolute Temperature Measurements at the Nanoscale. *Adv. Mater.* **2010**, *22*, 4499−4504.

(21) (a) Wade, S. A.; Collins, S. F.; Baxter, G. W. Fluorescence intensity ratio technique for optical fiber point temperature sensing. *J. Appl. Phys.* **2003**, *94*, 4743−4756. (b) Brites, C. D. S.; Lima, P. P.; Silva, N. J. O.; Millán, A.; Amaral, V. S.; Palacio, F.; Carlos, L. D. Thermometry at the nanoscale. *Nanoscale* **2012**, *4*, 4799−4829.

(22) (a) Rocha, J.; Brites, C. D. S.; Carlos, L. D. Lanthanide Organic Framework Luminescent Thermometers. *Chem. - Eur. J.* **2016**, *22*, 14782−14795. (b) Cui, Y. J.; Zou, W. F.; Song, R. J.; Yu, J. C.; Zhang, W. Q.; Yang, Y.; Qian, G. D. A ratiometric and colorimetric luminescent thermometer over a wide temperature range based on a lanthanide coordination polymer. *Chem. Commun.* **2014**, *50*, 719−721.

(23) Cui, Y. J.; Xu, H.; Yue, Y. F.; Guo, Z. Y.; Yu, J. C.; Chen, Z. X.; Gao, J. K.; Yang, Y.; Qian, G. D.; Chen, B. L. A Luminescent Mixed-Lanthanide Metal−Organic Framework Thermometer. *J. Am. Chem. Soc.* **2012**, *134*, 3979−3982.

(24) Cadiau, A.; Brites, C. D. S.; Costa, P. M. F. J.; Ferreira, R. A. S.; Rocha, J.; Carlos, L. D. Ratiometric Nanothermometer Based on an Emissive Ln^{3+}-Organic Framework. *ACS Nano* **2013**, *7*, 7213−7218.

(25) Zhao, S.-N.; Li, L.-J.; Song, X.-Z.; Zhu, M.; Hao, Z. M.; Meng, X.; Wu, L.-L.; Feng, J.; Song, S.-Y.; Wang, C.; Zhang, H.-J. Lanthanide Ion Codoped Emitters for Tailoring Emission Trajectory and Temperature Sensing. *Adv. Funct. Mater.* **2015**, *25*, 1463−1469.

(26) See http://en.wikipedia.org/wiki/CIE_1931_color_space for more details (accessed April 2, 2018).

(27) Rodrigues, M. O.; Dutra, J. D. L.; Nunes, L. A. O.; de Sá, G. F.; de Azevedo, W. M.; Silva, P.; Paz, F. A. A.; Freire, R. O.; A. Júnior, S. A. $Tb^{3+}\rightarrow Eu^{3+}$ Energy Transfer in Mixed-Lanthanide-Organic Frameworks. *J. Phys. Chem. C* **2012**, *116*, 19951−19957.

(28) Auzel, F. Upconversion and Anti-Stokes Processes with f and d Ions in Solids. *Chem. Rev.* **2004**, *104*, 139−174.

(29) Jongeneelen, F. J. A guidance value of 1-hydroxypyrene in urine in view of acceptable occupational exposure to polycyclic aromatic hydrocarbons. *Toxicol. Lett.* **2014**, *231*, 239−248.

(30) (a) Nagarkar, S. S.; Joarder, B.; Chaudhari, A. K.; Mukherjee, S.; Ghosh, S. K. Highly Selective Detection of Nitro Explosives by a Luminescent Metal−Organic Framework. *Angew. Chem., Int. Ed.* **2013**, *52*, 2881−2885. (b) Ramachandra, S.; Popović, Z. D.; Schuermann, K. C.; Cucinotta, F.; Calzaferri, G.; De Cola, L. Förster Resonance Energy Transfer in Quantum Dot-Dye-Loaded Zeolite L Nanoassemblies. *Small* **2011**, *7*, 1488−1494.

(31) (a) Schuster, M.; Meyer, W. H.; Wegner, G.; Herz, H. G.; Ise, M.; Schuster, M.; Kreuer, K. D.; Maier, J. Proton mobility in oligomer-bound proton solvents: imidazole immobilization via flexible spacers. *Solid State Ionics* **2001**, *145*, 85−92. (b) Li, G. H.; Lee, C. H.; Lee, Y. M.; Cho, C. G. Preparation of poly(vinyl phosphate-*b*-styrene) copolymers and its blend with PPO as proton exchange membrane for DMFC applications. *Solid State Ionics* **2006**, *177*, 1083−1090. (c) Karadedeli, B.; Bozkurt, A.; Baykal, A. Proton conduction in adipic acid/benzimidazole hybrid electrolytes. *Phys. B* **2005**, *364*, 279−284.

(32) (a) Yang, F.; Xu, G.; Dou, Y.; Wang, B.; Zhang, H.; Wu, H.; Zhou, W.; Li, J.-R.; Chen, B. A flexible metal−organic framework with a high density of sulfonic acid sites for proton conduction. *Nature Energy* **2017**, *2*, 877−883. (b) Kim, S.; Joarder, B.; Hurd, J. A.; Zhang, J.; Dawson, K. W.; Gelfand, B. S.; Wong, N. E.; Shimizu, G. K. H. Achieving Superprotonic Conduction in Metal−Organic Frameworks through Iterative Design Advances. *J. Am. Chem. Soc.* **2018**, *140*, 1077−1082.

(33) Zhou, L.-J.; Deng, W.-H.; Wang, Y.-L.; Xu, G.; Yin, S.-G.; Liu, Q.-Y. Lanthanide−Potassium Biphenyl-3,3′-disulfonyl-4,4′-dicarboxylate Frameworks: Gas Sorption, Proton Conductivity, and Luminescent Sensing of Metal Ions. *Inorg. Chem.* **2016**, *55*, 6271−6277.

(34) Liang, X. Q.; Zhang, F.; Zhao, H. X.; Ye, W.; Long, L. S.; Zhu, G. S. A proton-conducting lanthanide metal−organic framework integrated with a dielectric anomaly and second-order nonlinear optical effect. *Chem. Commun.* **2014**, *50*, 6513−6516.

(35) Bao, S.-S.; Otsubo, K.; Taylor, J. M.; Jiang, Z.; Zheng, L.-M.; Kitagawa, H. Enhancing Proton Conduction in 2D Co−La Coordination Frameworks by Solid-State Phase Transition. *J. Am. Chem. Soc.* **2014**, *136*, 9292−9295.

(36) Biswas, S.; Chakraborty, J.; Singh Parmar, V.; Bera, S. P.; Ganguli, N.; Konar, S. Channel-Assisted Proton Conduction Behavior in Hydroxyl-Rich Lanthanide-Based Magnetic Metal−Organic Frameworks. *Inorg. Chem.* **2017**, *56*, 4956−4965.

(37) Shigematsu, A.; Yamada, T.; Kitagawa, H. Wide Control of Proton Conductivity in Porous Coordination Polymers. *J. Am. Chem. Soc.* **2011**, *133*, 2034−2036.

NOTE ADDED AFTER ASAP PUBLICATION

This paper was published on the Web on June 19, 2018, with errors on the x-axes for Figures 2−4. The corrected version was reposted on July 2, 2018.

DOI: 10.1021/acs.inorgchem.8b00865
Inorg. Chem. 2018, 57, 7805−7814